CLINICAL ORTHOPAEDICS AND RELATED RESEARCH
Number 447, pp. 214–220

Comparison of Capacitive versus Resistive Joint Contact Stress Sensors

L. Martinelli, MSc; C. Hurschler, PhD†; and D. Rosenbaum, Prof. Dr.**

Cartilage contact stress elevations might be associated with pain or other symptoms after malunited, incongruous intraarticular fractures. Studies identifying fractures with patterns of elevated contact stresses would help to ensure more appropriate choices of treatment. However, appropriate instrumentation for such studies is crucial. We tested two such systems, one capacitive and one resistive, under identical loading conditions presumed to occur in the ankle. We used a materials testing machine and customized-loading fixtures to measure force detection error, contact area error, repeatability, homogeneity, creep, and one-axis and two-axis bending artifacts. The loading regimen caused pressures up to 2.5 MPa. An error in force detection between –3% and +5% was observed with the capacitive sensor whereas an error between –12% and +20% was observed with the resistive sensor. Repeatability and homogeneity were greater for the capacitive sensor. Errors in contact area measurement were less than 2% for the resistive sensor and less than 6% for the capacitive sensor. The resistive sensor could not conform to spherical surfaces without crinkling. Creep artifact was observed with both sensors. We concluded that the capacitive sensor had superior performance even though its thickness and high compliance may be disadvantageous in intraarticular measurements. The resistive sensor is required for use where higher pressures are expected despite its inferior accuracy.

Determining the magnitude and distribution of contact stress as a function of joint loading is important in understanding the pathogenesis of degenerative arthritis and other disorders such as unstable, injured, or surgically treated joints. Knowledge of the patterns of contact stresses in different injuries and treatments should allow comparison of approaches and choice of a specific approach to restore joint function.

The forces occurring in the ankle are approximately one to three times body weight for static and dynamic conditions, respectively.[7,9,14] Some authors reported ankle contact pressures obtained using Fuji film (Fujifilm Medical Systems USA, Inc, Stamford, CT), a static, passive technology which provides pressure only at one time under one set of circumstances.[1,10,11] Newer active pressure sensors allow continuous data collection during dynamic simulations of joint movements in vitro and in vivo.[14] These commercially available sensors are based on a resistive or capacitive technology. However, sensor performance depends on the test setup and laboratory conditions in which they operate. Artifacts, such as temperature drift, creep, and bending may affect overall sensor behavior with respect to accuracy and repeatability because of the nonstandard conditions in which sensors are used in laboratory experiments. To properly interpret studies using these techniques, it is crucial to understand their behaviors and limitations.

Therefore, we sought to determine the functional characteristics of the two sensors under identical loading conditions similar to those encountered in joint kinetic experiments. We asked the following questions: (1) what force errors occur in the two devices when measuring applied forces through flat and curved surfaces; (2) what errors in contact area measurements occur in the two sensors in various geometric configurations; (3) are the force measurements repeatable in the same test; (4) do the sensors show the same response to an applied load regardless of its location on the surface; (5) how are sensors affected by creep artifact; and (6) do sensors respond with the same accuracy when bent?

MATERIALS AND METHODS

The two sensors were based on different technologies: resistive and capacitive. The resistive Tekscan ISCAN® 5051 Sensor (Tekscan, Boston, MA) with a saturation pressure of 17.1 MPa

Received: April 4, 2005
Revised: November 18, 2005
Accepted: February 16, 2006
From the *Motion Analysis Laboratory, University Hospital Muenster, Muenster, Germany; and the †Laboratory for Biomechanics and Biomaterials, Department of Orthopaedics, Medical School of Hannover, Hannover, Germany.
Each author certifies that he or she has no commercial associations (eg, consultancies, stock ownership, equity interest, patent/licensing arrangements, etc) that might pose a conflict of interest in connection with the submitted article.
Correspondence to: Dieter Rosenbaum, Motion Analysis Laboratory, Orthopaedic Department, University Hospital Muenster, Domagkstr. 3 D-48149 Muenster, Germany. Phone: 49-0-251-83-52-970; Fax: 49-0-251-83-52-993; E-mail: diro@uni-muenster.de.
DOI: 10.1097/01.blo.0000218730.59838.6a

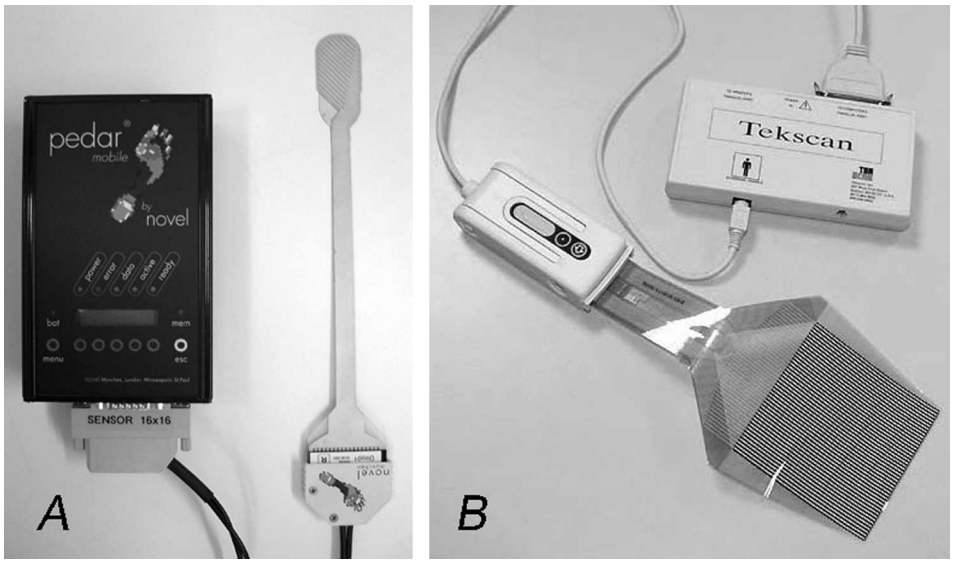

Fig 1A–B. The (A) Ankle Joint Pressensor (AJP) and (B) ISCAN® sensors are shown.

and the capacitive Novel AJP sensor (Novel GmbH, Munich, Germany) with a saturation pressure of 2.5 MPa were tested (Fig 1; Table 1).

The capacitive cells are created by a grid of conductive strips glued on an elastic dielectric material. Each intersection of two active strips results in a capacitor. Under external load, the dielectric thickness decreases, causing a change of the capacitance according to the equation:

$$C = \varepsilon\varepsilon_0 \cdot \frac{A}{d} \text{ (where } \varepsilon, \varepsilon_0 = \text{dielectric constants; } A = \text{plate area; and } d = \text{plate distance)}$$

The resistive sensor consists of two Mylar sheets that have electrically conductive electrodes deposited in varying patterns. Before assembly, a semiconductive coating (ink) is applied as an intermediate layer between the electrical contacts (rows and columns). This ink provides a change of the electrical resistance at each of the intersecting points when pressure is applied. When the two Mylar sheets are placed on top of each other, a grid pattern is formed, creating a sensing location at each intersection. By measuring the changes in current flow at each intersection, the applied force distribution pattern can be measured.

The technologies used to connect the resistor and capacitive sensor elements (sensels) to the signal-conditioning electronics are based on the same principle: a sensor matrix and a multiplexer which allows reading of the array of parallel sensor elements in a serial manner and displays two-dimensional pressure distribution in real time.

We used a materials testing machine (Zwick 005; Zwick & Co KG GmbH, Ulm, Germany) to apply repeatable loads to the sensors. The load cell allows for a maximum axial force of 5 kN with a precision of 0.4%. Protocols were written using software provided by the manufacturer (TestXpert® v.10.11). The machine can perform constant holding tests, cyclic loading, and stepwise loading for tension and compression. These methods were combined depending on the requirements needed. Known loads were applied to the two sensors using computerized numerically controlled machined surfaces and counter surfaces made of polyvinyl chloride (PVC) (construction precision, 10 μm). Three geometric configurations were used: flat (circular), spherical, and cylindrical (Fig 2; Table 2). Rigid steel indenters, not deformable at the pressure range used during testing, were used because the aim was to apply forces and not pressures, which would have required bladders. Small (area, 0.9 cm^2) and medium (area, 3.3 cm^2) flat indenters were used with different kinds of setups to cover a contact area ranging from 0.9 cm^2 to 6.6 cm^2 (Table 3). The cylindrical surfaces had radii of 40 mm (upper plate) and 50 mm (bottom plate); two pairs of spherical counter surfaces were used with radii of 30 mm and 50 mm, respectively. Curved surfaces were used to test sensors under deformation in different directions. Data from the force sensor of the materials testing machine and from the two sensors were compared. Loads were increased during a 5-second period, held for 10 seconds, and released over 5 seconds. Data were acquired after 5 seconds of the static condition. All tests were based on the same loading history. The setup of the test was comparable to the one described by Wilson et al[15] with respect to loading and unloading phases but, in contrast, did not use the silicone interface.

Before testing, calibration and preconditioning of the ISCAN® sensor were performed. First, three different forces (500 N,

TABLE 1. Technical Specifications of Sensors

Technical Specifications	AJP	ISCAN
Thickness (mm)	1	0.1
Dimensions (mm)	28 × 43	56 × 56
Resolution (sensels/cm^2)	16	62
Maximum pressure (MPa)	2.5	17.1

AJP = ankle joint pressensor

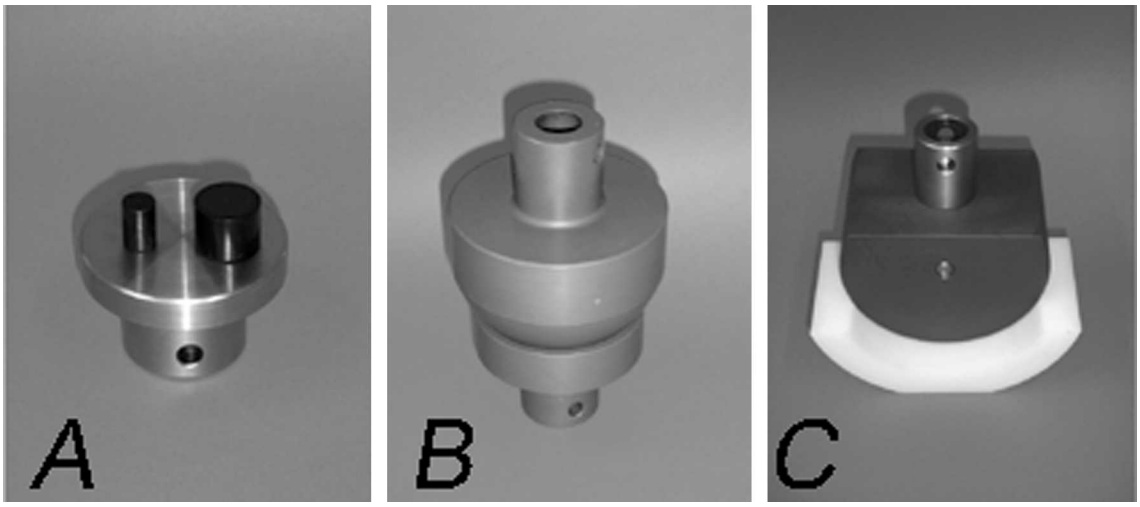

Fig 2A–C. The (A) flat, (B) spherical, and (C) cylindrical surfaces of the loading fixtures are shown.

1000 N, and 1500 N) were applied cyclically to the entire sensor surface. Once the sensor was preconditioned, it was calibrated. To distribute the load uniformly on the entire area, a silicone sheet was applied at the interface. Subsequently, the sensor was calibrated according to the manufacturer's protocol, during which calibration was performed at two force steps, which allowed generation of calibration curves based on a power law equation. According to the manufacturer of the ISCAN® sensor, the calibration loads can be applied only on a certain area of the sensor surface; the software presumes all the other sensels respond to the same load with a similar signal output. Therefore, a flat indenter (20 × 30 mm) was used to apply loads to the central part of the sensor. As an interface, a silicone sheet was used to distribute the load more uniformly across the ISCAN® sensor during the calibration procedure because otherwise nonhomogeneous loading, possibly with small areas of load saturation, would have occurred between the two rigid loading surfaces. The sensor was calibrated only on flat surfaces to investigate the potential error in force detection when the sensor was loaded in a bending situation. The two calibration values of 500 N (83 N/cm^2) and 1000 N (166 N/cm^2) represent 33% and 66% of the testing pressure range. The data were recorded after 5 seconds from the beginning of the holding time, which lasted for 30 seconds, to equilibrate the sensels. The ISCAN® system requires preconditioning and calibration each time a measurement is completed.

Calibration of the AJP sensor required the use of a pressure bladder. The sensor was placed under the bladder, which was inflated to reach the desired pressures. Ten pressure levels uniformly distributed between 4 N/cm^2 and 250 N/cm^2 were applied to the sensor to create a look-up table with capacitive values and pressure values. The software allows choosing the respective calibration data for a particular application. The AJP sensor should be calibrated approximately every 6 months.

The test evaluated the error in force detection when the load was applied with two different-sized cylindrical indenters. Error was defined as:

$$E_{force} = [(F_{sensor} - F_{loadcell})/F_{loadcell}] \times 100\%$$

with E_{force} being the error in force detection, F_{sensor} being the force value measured with the pressure sensors, and $F_{loadcell}$ as the force value measured with the load cell. The data from the sensors and the load cell were synchronized. Three forces, 100 N, 150 N, and 200 N, were applied using flat surfaces. The area of the flat plates was varied to accommodate for the entire pressure range of as much as 2.22 MPa, approximately the maximum pressure that can be measured with the AJP. Loads were applied in static and dynamic modes on three randomly selected areas of the sensor surface to investigate the homogeneity of the sensors. Each dynamic trial consisted of 10 cycles. Area values were calculated using the software provided by manufacturers. Error in area detection was defined as:

$$E_{area} = [(A_{sensor} - A_{ind})/A_{ind}] \times 100\%$$

TABLE 2. Load Surfaces and Applied Forces

Load Surface	Force (N)
Flat cylinder	100–150–200
Spherical	100
Cylindrical	600–1200–1800

TABLE 3. Pressures (in N/cm^2) Generated with Each Indenter and Corresponding Force Level

Area (cm^2)	Force 100 N	Force 150 N	Force 200 N
0.9	111	166	222
1.8	55	83	111
3.3	30	45	60
6.6	15	22	30

with E_{area} being the error in area detection, A_{sensor} being the area measured by the sensors, and A_{ind} the real area of the indenters.

The maximum force recorded during application of each static force loading was reported. The force error was calculated and plotted. Data from the same test settings of the two systems were compared.

Repeatability was defined as the standard deviation in a set of 10 repetitions and was investigated by analyzing the data collected in 10 repetitions performed at three force levels under the following conditions: flat cylinders, 100 N, 150 N, and 200 N; semicylindrical surfaces, 600 N, 1200 N and 1800 N; and spherical surfaces, 100 N – only AJP.

Three different positions were investigated using the flat cylinders. Recovery time was set to 30 seconds based on the result of a creep test.

Two semicylindrical surfaces were used, both made from PVC using a computerized numerically controlled machine, characterized by two different curvature radii (50-mm bottom plate, 40-mm top plate). The results of this test were analyzed to investigate a possible difference in force measurements when the sensors were bent uniaxially. The radii were chosen to transfer load to the central part of the sensors. The protocol included three force levels: 600 N, 1200 N, and 1800 N.

A potential limitation of pressure sensors is an inability to adapt to three-dimensional surfaces without crinkling. Fuji film must be cut into slices to improve conformity to curved surfaces,[2,6] whereas Tekscan and Novel technologies do not allow for such modification. Tekscan only allows for minimal external cutting to match the desired size or shape. To investigate the flexibility of the sensors, two spherical surfaces were used, which had radii of 50 mm and 30 mm. The mating spherical surfaces were fully conforming. The applied force was 100 N.

Creep is an important parameter negatively influencing the results of a test because it limits the cycle frequency. Creep (C_r) was defined as the change in output under a static load.

$$C_r = E_{force} \text{ (after 300s)} = E_{force} = [(F_{sensor} - F_{loadcell})/F_{loadcell}] \times 100\%$$

Sinusoidal loads applied with a period less than the time needed for sensor recovery will produce a creep artifact. Both technologies are affected by such artifact; this test aimed to determine to what degree. We chose peak force during the static trial as the parameter chosen for determining creep. In an analysis of the reliability of the Pedar system (Novel GmbH, Munich, Germany),[4] the peak force had the highest intraclass correlation coefficient, and therefore was considered an acceptable parameter for this analysis. The raw data collected during the test were plotted to conduct a first visual control of the error trend. The interval between each data sample was 30 seconds. After visual control of various curve-fitting algorithms, a second-order polynomial curve was chosen to represent the raw plots of the 10 points to describe the creep during a 300-second period. The applied load was 200 N, resulting in 2 MPa. Two 300-second cycles were applied with different recovery intervals to investigate the time needed by the sensors to recover from the previous loading event (memory artifact). The force was transferred using the medium-sized PVC cylinder. The two error trends were compared and plotted.

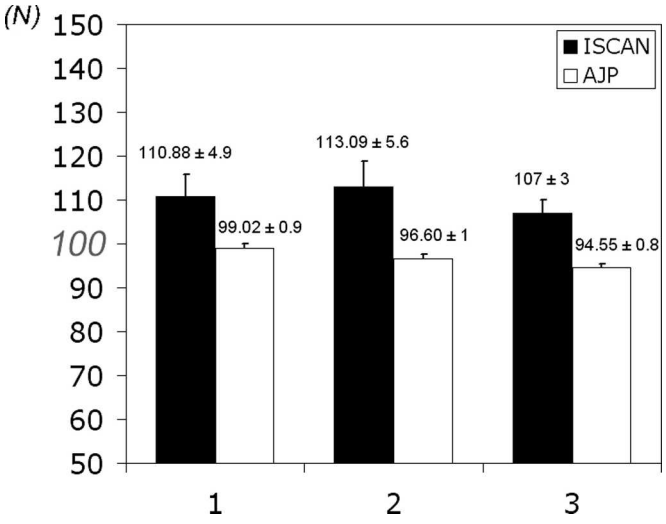

Fig 3. Force detection accuracy with flat surfaces at the three load positions with a mean (SD) of 10 repetitions in each position is shown (100 N = applied load level; 0.6 MPa). The results indicate the AJP slightly underestimates the forces whereas the ISCAN® reports higher force errors.

RESULTS

The maximum force error (E_{force}) was lower for the AJP (range, −3% to +5%) as compared with the ISCAN® system (range, −12% to +20%) over all the force levels investigated (Figs 3–5).

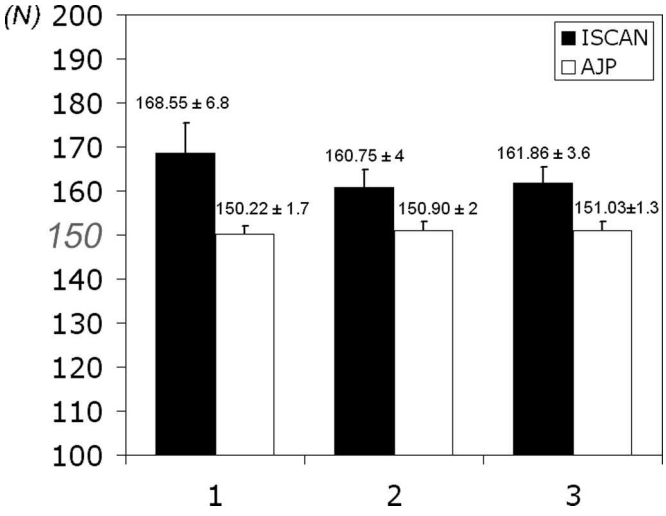

Fig 4. Force detection accuracy with flat surfaces at three load positions with a mean (SD) of 10 repetitions in each position is shown (150 N = applied load level; 1.66 MPa). The results show little deviation of the forces reported by the AJP whereas the ISCAN® reveals higher force errors.

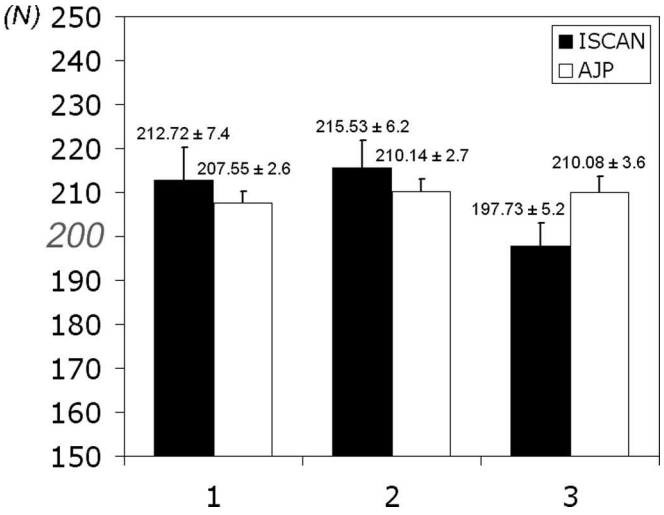

Fig 5. Force detection accuracy with flat surfaces at three load positions with a mean (SD) of 10 repetitions in each position is shown (200 N = applied load level; 2.22 MPa). The results show the forces reported by the AJP and the ISCAN® are higher than the applied force, but the error is more pronounced for the ISCAN® (with the exception of the ISCAN® value for Position 3, which slightly underestimated the force).

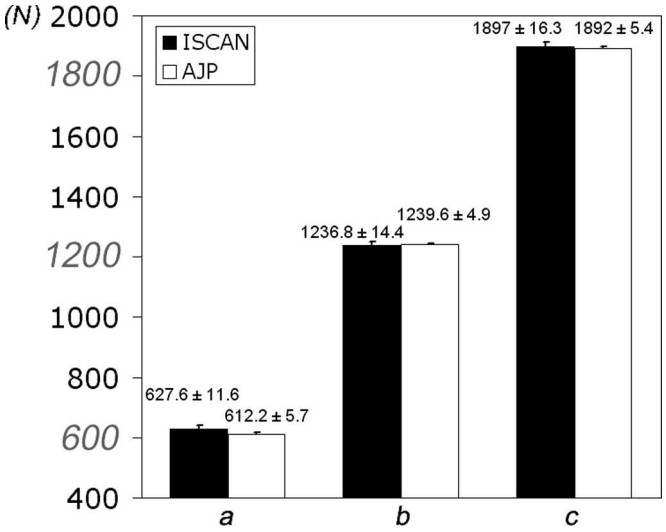

Fig 6. Force detection with cylindrical surfaces with a mean (SD) of 10 repetitions for each force level is shown (applied load levels were 600 N, 1200 N, and 1800 N, respectively). The errors reported by the AJP and the ISCAN® sensor are comparable but the standard deviation is greater for the ISCAN® system, indicating a reduced repeatability.

The ISCAN® system had an area error (E_{area}) of 2%, whereas the error of the AJP depended on the total area applied and on the position on the sensor. The error was within 6% for areas between 3.3 cm^2 and 6.6 cm^2. We observed lower sensor accuracy in area detection of smaller areas, where E_{area} of as much as 20% were observed. To decrease this error, we developed a protocol to reduce the error to 6%. The protocol excluded partially loaded cells from the area determination process, and the sensor threshold was increased according to the curve area error/threshold. Because of its stiffness, the ISCAN® reported lower area values when loads were applied without the silicone interface where incongruencies in the contact surface can result in unloaded areas under the indenter.

The repeatability was better for the AJP system for flat and cylindrical surfaces (Table 4). The ISCAN® did not perform accurately in the 10-cycles loading test. For the ISCAN® sensor, different force detection errors depended on the location of load application (Figs 3–5). That is, the E_{force} was related to the position of the applied load on the sensor surface and sensor homogeneity was low.

TABLE 4. Ranges of Standard Deviations (N)

Sensor	Flat Surfaces	Cylindrical Surfaces	Spherical Surface
ISCAN	3–7.4	11.6–16.3	/
AJP	0.8–3.6	4.9–5.7	3.8–3.9

The E_{force} in the cylindrical load setup was within 8% for the AJP and 9% for the ISCAN® (Fig 6). Even though the AJP is characterized by a greater thickness, the load distribution was comparable with the ISCAN® distribution. We recorded no differences between directions of curvature.

The AJP had an E_{force} of 8% with the 50-mm radius sphere and 12% with the 30-mm sphere (Fig 7). The

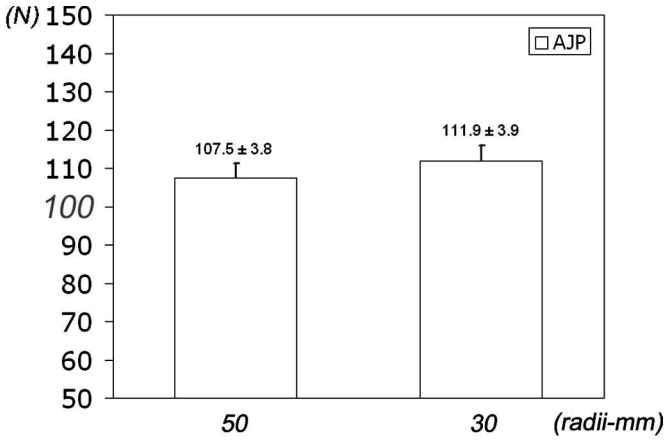

Fig 7. Force detection accuracy with spherical surfaces with a mean (SD) of 10 repetitions for each radius of 30 mm and 50 mm is shown (100 N = applied load level). The results indicate the force error is under three-dimensional loading is approximately 10% and is higher with a more pronounced curvature.

ISCAN® showed crinkle artifact during pretesting with spherical surfaces. Therefore, the spherical surfaces were not used with the ISCAN® system because the radii of the spherical contact surfaces were too small to allow loading without large crimps and potential sensor damage.

Creep artifact (C_r) was 16% for the AJP and 18% for the ISCAN® sensor. Memory artifact was recorded after the unloading time of 15 seconds for the ISCAN® system. After 30 seconds of relaxation, no artifact remained to affect subsequent measurements.

DISCUSSION

The Tekscan ISCAN® is a widely used technology in pressure and/or force detection applications. Several studies purport to validate this technology.[3,5,8,15] The AJP is the first capacitive sensor developed specifically for ankle investigations. The comparison between these technologies was intended to help investigators make informed decisions regarding applicability and limitations of the two systems.

Certain limitations have to be mentioned. Sensors were not tested in an actual ankle or ankle prosthesis, but were tested in a simplified mechanical setup with different indenters and surfaces to simulate the range of potential loading conditions. This approach was chosen deliberately to ensure the comparability of the two sensors. For the same reason, to compare both sensors under identical loads, the investigated pressure range was in the lower range of the ISCAN® sensor. Therefore, the results are applicable for the specified load range only.

The ISCAN® force detection error (E_{force}) using flat surfaces was between -12% and +20%. The conditions of our test that were not ideal were attributable to the applied loads not corresponding exactly to calibration values and the loadings being at the lower end of the load range of the ISCAN® sensor.[8] The two pressure values of the calibration process were in the middle of testing pressure values.

The two sensors at first glance have different mechanical and shape characteristics. The different materials used for construction, Mylar for ISCAN® and foam rubber for AJP, likely explain the mechanical discrepancies. The stiffness of the ISCAN® film does not allow the sensor to be bent in two directions when placed between spherical surfaces. However, the AJP sensor could bend and conform to the surfaces, although this was associated with a maximum error of 12% in force detection. The lower E-modulus characterizing the dielectric and the overall size of the AJP sensor (28 mm x 45 mm) compared with the ISCAN® sensor (56 mm x 56 mm) explain the AJP sensor's greater flexibility.

Creep had a similar influence on both systems. The load-drifting curve, generated using a polynomial approximation, is in accordance with the results reported by Otto et al.[8] The ISCAN® needed a longer unloading period between two cycles to recover to its original state.

The overall sensor performances may be influenced by the different calibration processes. The main difference between the two systems is the reference parameter used to calibrate the ISCAN® is not pressure, as for the AJP, but force. Additionally, ISCAN® software averages across all sensels assuming similar properties, whereas the AJP calibration considers the individual characteristics of all sensels in the process.

The repeatability was greater for the AJP especially because the ISCAN®'s precision depends on the area where load is applied. In previous tests, a force error was reported up to 6.5% for flat surfaces and 31% when cemented.[15] The test protocols were comparable to those used by Wilson et al,[15] but we did not use a silicone interface. With the silicone approach, loads are better distributed over the sensor surface, avoiding possible errors because of out-of-range pressure peaks. However, we decided not to use an interface to reproduce the test condition of a joint prosthesis and rather to apply loads randomly on the entire sensor surface; this resulted in overestimated forces in the center part of the ISCAN®, and underestimated forces near the borders. This problem could interfere with accuracy when the contact area is not known before sensor placement.

However, the ISCAN® sensor, because of its higher spatial sensel resolution, has an E_{area} of only 2%. The lower spatial resolution of the AJP highly compromised the contact area measurements when using indenters smaller than 3 cm^2. The protocol applied to the dataset allowed reducing the error to an average of 6%. Drawbacks of this approach are the need of postanalysis and possible exclusion of data in the lower pressure range through the use of a correction algorithm as described above.

Although the ISCAN® is reusable, our experience has shown its lifetime is influenced by the severity of the loading conditions. The ISCAN® has the advantage of being only 0.1 mm thick, which is 10 times less than the 1-mm thickness of the AJP. The AJP's dielectric thickness results in more uniform redistribution of loading, which may not represent the actual loading of the joint being measured.

The AJP sensor had a better repeatability and behaved more uniformly across the whole sensor area in the investigated pressure range, which admittedly was not optimal for the ISCAN® sensor, representing the lower 15% of its load range. The ISCAN® sensor measured area more accurately. The decision as to which system to use for a given application should be based on the magnitude of the expected loading and the relative importance of accuracy,

repeatability, and conformability to complex geometric features of the given application. Accuracy, repeatability, and conformability are attained at the cost of resolution and potentially biased area and peak pressure measurements using the thicker AJP sensor, and improved area and pressure distribution measurements at the cost of accuracy and repeatability when using the thinner ISCAN® sensor.

References

1. Bertsch C, Rosenbaum D, Claes L. Intra-articular and plantar pressure distribution of the ankle joint complex in relation to foot position. *Unfallchirurg*. 2001;104:426–433.
2. Brown TD, Rudert MJ, Grosland NM. New methods for assessing cartilage contact stress after articular fracture. *Clin Orthop Relat Res*. 2004;423:52–58.
3. Harris ML, Morberg P, Bruce WJ, Walsh WR. An improved method for measuring tibiofemoral contact areas in total knee arthroplasty: a comparison of K-scan sensor and Fuji film. *J Biomech*. 1999;32: 951–958.
4. Kernozek TW, LaMott EE, Dancisak MJ. The reliability of an in-shoe pressure measurement system during treadmill walking. *Foot Ankle Int*. 1996;17:204–207.
5. Luo ZP, Berglund LJ, An KN. Validation of F-scan pressure sensor system: a technical note. *J Rehabil Res Dev*. 1998;35:186–191.
6. MacKenzie JR, Callaghan JJ, Pedersen DR, Brown TD. Areas of contact and extent of gaps with implantation of oversized acetabular components in total hip arthroplasty. *Clin Orthop Relat Res*. 1994; 298:127–136.
7. Nuber GW. Biomechanics of the foot and ankle during gait. *Clin Podiatr Med Surg*. 1989;6:615–627.
8. Otto JK, Brown TD, Callaghan JJ. Static and dynamic response of a multiplexed-array piezoresistive contact sensor. *Experimental Mechanics*. 1999;39:317–323.
9. Procter P, Paul JP. Ankle joint biomechanics. *J Biomech*. 1982;15: 627–634.
10. Rosenbaum D, Bertsch C, Claes L. Tenodeses do not fully restore ankle joint loading characteristics: a biomechanical in vitro investigation in the hind foot. *Clin Biomech (Bristol, Avon)*. 1997;12: 202–209.
11. Rosenbaum D, Eils E, Hillmann A. Changes in talocrural joint contact stress characteristics after simulated rotationplasty. *J Biomech*. 2003;36:81–86.
12. Sammarco GJ, Burstein AH, Frankel VH. Biomechanics of the ankle joint. *Orthop Clin North Am*. 1973;4:75–96.
13. von Eisenhart-Rothe R, Witte H, Steinlechner M, Muller-Gerbl M, Putz R, Eckstein F. Quantitative determination of pressure distribution in the hip joint during the gait cycle. *Unfallchirurg*. 1999;102: 625–631.
14. Wasielewski RC, Galat DD, Komistek RD. Correlation of compartment pressure data from an intraoperative sensing device with postoperative fluoroscopic kinematic results in TKA patients. *J Biomech*. 2005;38:333–339.
15. Wilson DR, Apreleva MV, Eichler MJ, Harrold FR. Accuracy and repeatability of a pressure measurement system in the patellofemoral joint. *J Biomech*. 2003;36:1909–1915.